Available online at www.sciencedirect.com
ScienceDirect
Journal of Power Sources 160 (2006) 835–841
JOURNAL OF POWER SOURCES
www.elsevier.com/locate/jpowsour

MCFC and microturbine power plant simulation

F. Orecchini, E. Bocci *, A. Di Carlo

CIRPS-Interuniversity Research Centre for Sustainable Development, University of Rome "La Sapienza", Italy

Available online 12 June 2006

Abstract

The consistent problem of the CO_2 emissions and the necessity to find new energy sources, are motivating the scientific research to use high efficiency electric energy production's technologies that could exploit renewable energy sources too. The molten carbonate fuel cell (MCFC) due to its high efficiencies and low emissions seems a valid alternative to the traditional plant. Moreover, the high operating temperature and pressure give the possibility to use a turbine at the bottom of the cells to produce further energy, increasing therefore the plant's efficiencies. The basic idea using this two kind of technologies (MCFC and microturbine), is to recover, via the microturbine, the necessary power for the compressor, that otherwise would remove a consistent part of the MCFC power generated. The purpose of this work is to develop the necessary models to analyze different plant configurations. In particular, it was studied a plant composed of a MCFC 500 kW Ansaldo at the top of a microturbine 100 kW Turbec. To study this plant it was necessary to develop: (i) MCFC mathematical model, that starting from the geometrical and thermofluidodynamic parameter of the cell, analyze the electrochemical reaction and shift reaction that take part in it; (ii) plate reformer model, a particular compact reformer that exploit the heat obtained by a catalytic combustion of the anode and part of cathode exhausts to reform methane and steam; and (iii) microturbine-compressor model that describe the efficiency and pressure ratio of the two machines as a function of the mass flow and rotational regime. The models developed was developed in Fortran language and interfaced in Chemcad© to analyze the power plant thermodynamic behavior. The results show a possible plant configuration with high electrical and global efficiency (over 50 and 74%).

Keywords: Modelling; MCFC; Microturbine; MIR

1. Introduction

Different kinds of fuel cells characterized by high efficiency and environmental compatibility are under development at the moment. In particular, the technology of molten carbonate fuel cells (MCFCs) is now at the stage of scale up to commercialization and many developers have shown significant progresses. MCFCs are planar cells formed by a matrix (tile) filled with carbonates and coupled with two electrodes where the following reactions occur:

$$H_2 + CO_3^{2-} \Rightarrow H_2O + CO_2 + 2e^- \text{ (A)} \quad (1)$$

$$\frac{1}{2}O_2 + CO_2 + 2e^- \Rightarrow CO_3^{2-} \quad \text{(C)} \quad (2)$$

On the anodic side, the water gas shift reaction occurs too:

$$H_2O + CO \Leftrightarrow H_2 + CO_2 \text{ (A)} \quad (3)$$

The fuel and the oxidant gases are fed separately, and the tile prevents gas crossover and guarantees an adequate ionic conduction and electronic insulation. To supply higher power, MCFCs are used superimposed in stacks, where cells are electrically connected in series and separated from each other by bipolar plates, also accomplishing the gas distribution.

High temperature fuel cells, such as molten carbonate fuel cells have the following advantages:

1 No need for expensive and easily poisoning catalysts (Pt based).
2 High operating temperature (about 923 K) which enables efficient recovery of residual pressure and waste heat via gas turbine bottoming cycle and cogeneration.

But focusing the attention in the energy production process exclusively on fuel cells is very restrictive since they cannot produce power on their own due to the fact that hydrogen in nature is not present in enough quantity. Therefore, the fuel must be obtained from primary sources, which at present time are mainly fossil fuels (e.g. oil or natural gas). For this reason a

* Corresponding author. Tel.: +39 0644585310; fax: +39 064881759.
E-mail address: enrico.bocci@uniroma1.it (E. Bocci).

0378-7753/$ – see front matter © 2006 Elsevier B.V. All rights reserved.
doi:10.1016/j.jpowsour.2006.04.094

Nomenclature

a,b	constant Table 5.
Cp	specific heat, J mol^{-1} K^{-1}
d	channel height, m
E	Nernst potential
E_j	activation energy, J mol^{-1}
F	Faraday's constant, C mol^{-1}
G	mass flowrate on compressor and turbine
h	heat transfer coefficient, kW m^{-2} K^{-1}
ΔH	formation enthalpy, J mol^{-1}
J	current density, A m^{-2}
K	constant in Table 1 or abs. rate in Table 4
n	gas flow rate, mol m^{-1} s^{-1}
n_c	rotational regime
n_e	electrons transferred in reactions (1) and (2)
P	pressure, atm
r	reaction rate, mol m^{-2} s^{-1}
R_Ω	electrode internal resistance m^2
R_{tot}	electrode total resistance m^2
s	cell component thickness, m
S	specific gas/solid interface area, m^2 m^{-2}
T	temperature, K
v	gas velocity, m s^{-1}
V	voltage, V
A, B, Cir, D, F	kinetic parameters in total resistance expression

Greek letters

β	compressor–expansion ratio
Ω	catalyst surface
λ	thermal conductivity
η	efficiency
ρ	density

Index

0	ideal condition adimensional
a	anode
c	cathode
cb	catalytic burner
comp	compression
esp	expansion
i	chemical species
j	reaction
n	component
ref	reformer
s	solid

reforming unit is needed to convert primary fuels in hydrogen, which can later be fed to the fuel cells.

Different studies and hypothesis were proposed to integrate high temperature fuel cells and gas turbine [1–3]. In [1], the predicted performance for a 220 kW, pressurized SOFC directly coupled with a micro gas turbine is reported. The hybrid cycle shows 57% expected electrical efficiency. Ref. [2] reports performance predicted for a 20 MW, ambient pressure, and internal reforming MCFC-based power plant fuelled with natural gas. In that case, the gas turbine is coupled with the fuel cells via heat exchangers and the expected electrical efficiency of the system is about 75%. Similar results are stated for 1 MW size on [3]. On the other hand, the processes reported in the literature are very different both for the fuel cell technology used and for the system configuration adopted. Therefore, a direct comparison cannot be made and also a comparison-based only on the expected electrical efficiency can be confusing. Furthermore, some extrapolation and simplification of the models have been made in particular when MW ranges are considered. The aim of this work is to study a particular power plant composed of a MCFC Ansaldo 500 kW coupled whit a microturbine TurbecT100 100 kW. Similar jobs are showed in [4]. The principal difference between this job and [4] are the models used for the MCFC and modular integrated reformer (MIR). In fact the MCFC model used for this job is a 2D model on the cell's plane. The choice of this more complicated model is owing to the need to take under control the local temperature on the cell's plane that have to be lower than 983 K. This is the maximum temperature admitted to avoid electrolyte evaporation and thermal corrosion. Another difference is the model used for the reformer, in fact, in this job a kinetic approach was adopted because it is reputed that in this way it is possible to obtain a better understanding of the reformer reactions behavior. A numerical steady-state simulation of the process is set up and detailed models of the components is developed in Fortran 90 and interfaced with Chemcad© software.

2. Mathematical models

2.1. MCFC model

The fuel cell model is two-dimensional on the horizontal cell plane, while temperature variations along the vertical coordinate are neglected. The model geometry was divided in three distinct zones: a planar solid zone (**S**) comprehensive of the two electrodes, the bipolar plate and the electrolytic matrix invested by the two crossflow gaseous stream (Anodic **A** and Cathode **C**). The model is based on the following hypotheses: (1) steady state conditions; (2) uniform voltage on the fuel cell plane; (3) adiabatic conditions; (4) no radiation heat exchanges between solid components and gas streams; (5) continuous description of the gas flow (distributed into a number of discrete channels) in terms of a specific rate of reactants per unit length of the fuel cell side; (6) fully developed velocity and temperature profiles in the gas streams; (7) plug-flow balance equations for the gas streams; and (8) thermodynamic equilibrium for shift reaction at the anode. Hypothesis (2) is justified by the high electrical conductivity of the current collectors; assumption (4) is explained by the consideration that (gases being nearly transparent in the infrared region) convective heat transfer is much greater than adsorption and radiation between gases and solid. Moreover, being the Reynolds number of the channels less than 100 and the Peclet number higher or much higher than 20, the plug-flow form of mass and energy balances of the gaseous streams (hypothesis 7) is fully justified.

Table 1
MCFC equations

Mass balance		
(Eq. (1))	**A**	$\frac{\partial n_i}{\partial x} = r_i \quad \text{where} \quad r_i = \sum_i \nu_{ij} r_j \, j = 1,3 \quad r_1 = \frac{J}{n_e F}$
(Eq. (2))	**C**	$\frac{\partial n_i}{\partial y} = r_i \quad \text{where} \quad r_i = \nu_{i2} r_2 \quad \text{and} \quad r_2 = r_1$
Energy balance		
(Eq. (3))	**A**	$\sum_i \frac{\partial (n_i Cp_i T_a}{\partial x} = \left(\sum_{Pi} \frac{\partial n_{Pi}}{\partial x} Cp T_s - \sum_{Ri} \frac{\partial n_{Ri}}{\partial x} Cp T_a \right) + h_a (T_s - T_a)$
(Eq. (4))	**C**	$\sum_i n_i Cp_i \frac{\partial T_c}{\partial y} = \sum_i \frac{\partial n_i}{\partial y} Cp_i T_c + h_c (T_s - T_c)$
(Eq. (5))	**S**	$h_c (T_s - T_c) + h_a (T_s - T_a) = Q_{\text{cond}} + Q_{\text{reaz}} \quad \text{where} \quad Q_{\text{cond}} = \sum_n \lambda_n S_n \left(\frac{\delta^2 T_s}{\delta x^2} + \frac{\partial^2 T_s}{\partial y^2} \right) \quad Q_{\text{reaz}} = \sum_{j=1}^{3} r_j \Delta H_j - VJ$
Momentum balance		
(Eq. (6))	**A**	$\frac{\partial p_a}{\partial x} = K_a \frac{\mu_a v_a}{d^2}$
(Eq. (7))	**C**	$\frac{\partial p_c}{\partial y} = K_c \frac{\mu_c v_c}{d^2}$
Electrochemical reactions		
(Eq. (8))	**S**	$E = E_0 - \frac{\text{RT}_s}{n_e F} \ln \left(\prod_i p_i^{\nu_i} \right)$
(Eq. (9))	**S**	$R_{\text{tot}} = A \frac{e^{B/T_s}}{\prod_i p_i^{\beta_i}} + R_\Omega + D e^{F/T_S}$
(Eq. (10))	**S**	$V = E - R_{\text{tot}} J$

The equations used are shown in Table 1. Mass, energy and momentum balances of the gaseous streams are included in the model, together with the energy balance of the solid. In particular, the rate of each "*j*" reaction (r_j) has been calculated on the basis of Faraday's law (reactions (1) and (2)) and shift equilibrium condition (reaction (3)). Owing to the laminar regimen in the gas channels, momentum balance is a linear function of gas velocity (Eq. (6) and (7)). The local kinetics is evaluated by subtracting the uniform fuel cell voltage from the local thermodynamic voltage (evaluated on the basis of the Nernst equation (Eq. (8))). The voltage losses are related to the electrical current through the local value of the resistance (Eq. (10)). The local resistance is evaluated using a semi-empirical model (Eq. (9)) as deducted by [5], function of the temperature. The parameters involved in the model have been chosen on the basis of the fuel cell geometry (*S*, *d*, *s*), of the materials involved (λ), of the flow regime (*h*) and of experimental data evaluated by Ansaldo ($K_a = 22$, $K_c = 46$). Finite difference method has been used for the numerical solution of the differential equation systems, together with relaxation method for the energy balance of the solid, which is a Fourier problem. The computer code has been developed in Fortran software and then interfaced in Chemcad©. The simulation results are the maps of gas and solid temperatures, electrical current density, Nernst voltage, polarization, internal resistance, pressure drops and compositions of the gaseous streams on the fuel cell plane.

2.2. MIR model

The modular integrated reformer (MIR) is a particular kind of plate reformer. Differently to the conventional tubular reformer the heating exchange surface is a plate so to make the reactor's dimension more compact. The particular geometry allow to reduce the reactor's length, so to limit the pressure losses too, giving the possibility to the reactor to work at 350 kPa, with better reforming efficiency. Thanks to the thin catalyst layer, this kind of reactor then allows faster start-up and faster loads changes [6]. Its geometry allows assembling the plates in stack so to make it still more compact. A typical scheme of this reactor is shown in Fig. 1.

The reactions that occur in the reformer are showed below:

Ref.

$$CH_4 + H_2O \Leftrightarrow CO + 3H_2 \tag{4}$$

$$CO + H_2O \Leftrightarrow CO_2 + H_2 \tag{5}$$

$$CH_4 + 2H_2O \Leftrightarrow CO_2 + 4H_2 \tag{6}$$

Burn.

$$H_2 + \frac{1}{2}O_2 \Rightarrow H_2O \tag{7}$$

$$CH_4 + 2O_2 \Rightarrow CO_2 + 2H_2O \tag{8}$$

$$CO + \frac{1}{2}O_2 \Rightarrow CO_2 \tag{9}$$

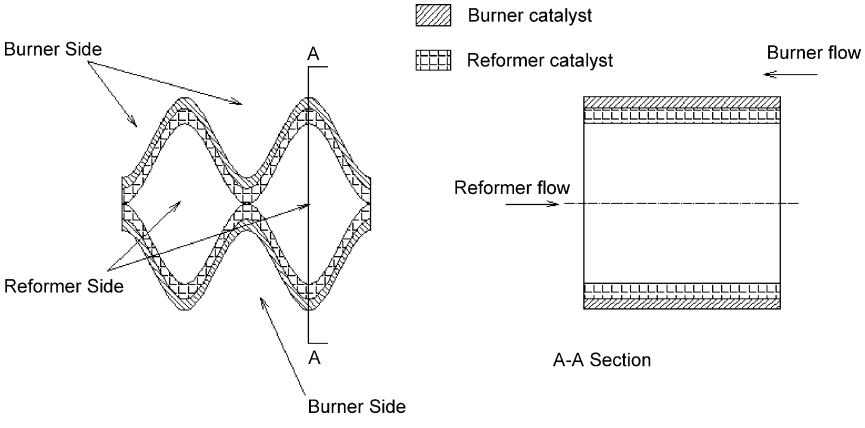

Fig. 1. Scheme of a reformer plate.

Table 2
Arrhenius for rate of reforming

Reaction	A (kmol kg_{cat}^{-1} s^{-1})	E (kJ mol^{-1})
(4)	3.72×10^{14} $Pa^{0.5}$	240
(5)	5.48×10^{7} Pa^{1}	67.13
(6)	8.99×10^{13} $Pa^{0.5}$	243.9

Table 3
Arrhenius for absorption rate

Species	A (Pa^{-1})	E (kJ mol^{-1})
CH_4	6.58×10^{-9}	−38.28
CO	8.14×10^{-10}	−70.65
H_2	6.05×10^{-14}	−82.9
H_2O	1.78×10^{10} Pa	88.68

To describe the reaction rate typical Arrenhius formula were used. The activation energy and the pre-exponential factor to complete define the reaction rate under Ni/Al_2O_3 catalyst are deducted from [7] and are described in Tables 2 and 3.

The following hypothesis was done: (1) steady state conditions; (2) complete combustion on the burner side; (3) no NO_x produced; (4) no diffusion limit on the reformer side; (5) ideal gas law whit c_p polynomial function of temperature; and (6) one dimensional model on the progress axis of reaction. The equations used to define the reactor's behavior are shown in Table 4.

Table 4
MIR equations

Mass balance on reformer side

$$\frac{\partial n_i}{\partial x} = \rho_{cat}\Omega r_i \quad \text{with} \quad r_i = \sum_j \nu_{ij} r_j$$

$$r_1 = \frac{k_1}{P_{H_2}^{2.5}}\left(P_{CH_4}P_{H_2O} - \frac{P_{H_2}^3 P_{CO}}{K_{eq1}}\right) \times \frac{1}{Q_r^2} \quad \text{with} \quad k_1 = A_1 e^{-Ea1/RT}$$

$$r_2 = \frac{k_2}{P_{H_2}}\left(P_{CO}P_{H_2O} - \frac{P_{H_2}P_{CO_2}}{K_{eq2}}\right) \times \frac{1}{Q_r^2} \quad \text{with} \quad k_2 = A_2 e^{-Ea2/RT}$$

$$Q_r = 1 + K_{CO}P_{CO} + K_{H_2}P_{H_2} + K_{CH_4}P_{CH_4} + \frac{K_{H_2O}P_{H_2O}}{P_{H_2}}$$

Energy equations

$$(R)\sum_i \frac{\partial n_i Cp_i(T_{ref})T_{ref}}{\partial x} = h_{ref}(T_{cb} - T_{ref}) + \sum_j r_j \Delta H_j$$

$$(B)\sum_i \frac{\partial n_i Cp_i(T_{cb})T_{cb}}{\partial x} = h_{cb}(T_{ref} - T_{cb})$$

2.3. Turbec T100

To define the turbine and compressor model it was necessary to build a mathematical model of the machine characteristic's (efficiency versus mass flow and pressure ratio versus mass flow as function of the two machine inlet temperature, rotational regime and mass flow). The model used is shown in Table 5.

2.4. Flow-sheet and simulation

Fig. 2 reports a general simulated plant flow sheet. Natural gas, after a primary treatment, is mixed with steam, pre-heated

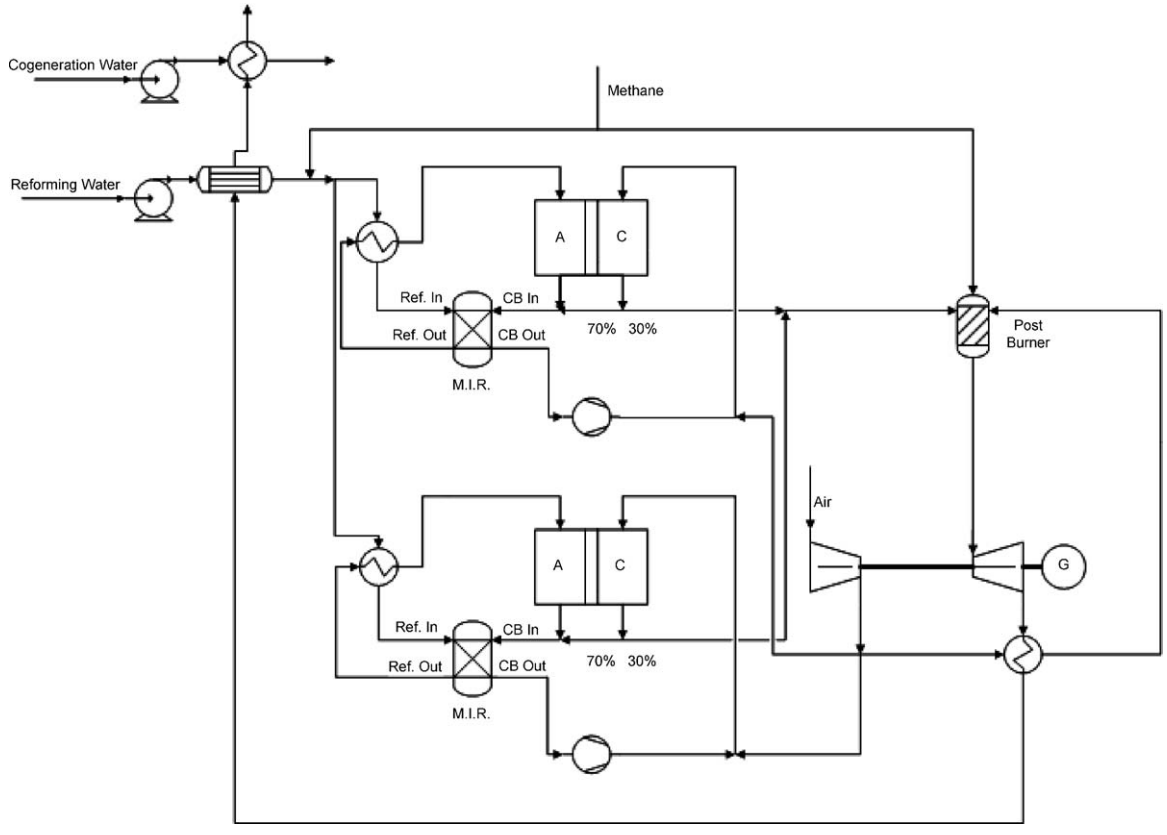

Fig. 2. Plant's flowsheet.

Table 5
Turbec T100 model used

Compressor
$\dot{\beta}_{\text{comp}} = c_1(\dot{n}_c)\dot{G}^2 + c_2(\dot{n}_c)\dot{G} + c_3(\dot{n})$
$\dot{\eta}_{\text{comp}} = [1 - c_4(1-\dot{n}_c)^2]\left(\frac{\dot{n}_c}{\dot{G}}\right)\left(\frac{2-\dot{n}_c}{\dot{G}}\right)$
where
$c_1(\dot{n}_c) = \frac{\dot{n}_c}{a(1-b/\dot{n}_c)+\dot{n}_c(\dot{n}_c-b)^2}$
$c_2(\dot{n}_c) = \frac{(a-2b\dot{n}_c^2)}{a(1-b/\dot{n}_c)+\dot{n}_c(\dot{n}_c-b)^2}$
$c_3(\dot{n}_c) = \frac{ab\dot{n}_c-b^2\dot{n}_c^3}{a(1-b/\dot{n}_c)+\dot{n}_c(\dot{n}_c-b)^2}$
$c_4 = 0.4$
Turbine
$\frac{G}{G_0} = \sqrt{1+t_1-\frac{t_1 n_c}{n_{c0}}}\sqrt{\frac{T_{\text{in0}}}{T_{\text{in}}}}\left(1-\left(\frac{\beta_{\text{esp}}-1}{\beta^*-1}-1\right)^2\right)$
$\eta_{\text{esp}} = [1-t_3(1-\dot{n}_t)^2]\left(\frac{\dot{n}_t}{\dot{G}}\right)\left(\frac{2-\dot{n}_t}{\dot{G}}\right)$
$t_3 = 0.4$

Table 6
Input specifications

Stacks	4
Cells per stacks	150
Maximum local T (K)	983
Steam/methane ratio	3
Fuel utilization (%)	75
Anhode inlet T (K)	873
Steam reformer inlet T (K)	443
Operative pressure (kPa)	350

in a regenerative heat exchanger and fed to the reformer, where CO and H_2 are produced. Exit gases passes again through regenerative exchanger, set ready to be processed at the anodic side of the fuel cells stack. After electrochemical and gas shift conversion, residual concentration of fuel is still present. In fact CH_4 not converted in the reformer pass inert in the stack and not all H_2 and CO is consumed. So fuel, containing effluent, is mixed with part of cathode exhausts and feed a catalytic burner where the heat necessary for endothermic reactions, taking place in reforming process, is produced and directly exchanged. Hot and CO_2 rich gas, exhaust of the combustor's side, is mixed with fresh air coming from compressor and fed to the cathode where O_2 and CO_2 are consumed by the electrochemical reaction. Part of cathode exhaust gas is sent to a turbine for recovering residual energy, which is used to drive air compressor and to produce further electrical energy. The hot effluent finally releases the heat necessary to produce steam for the reforming reaction and for cogeneration.

In order to have a reference to compare the results of the different simulations runs, the set of boundary conditions reported in Table 6 has been selected. They represent proper operating conditions for the present technology of MCFC stacks and are

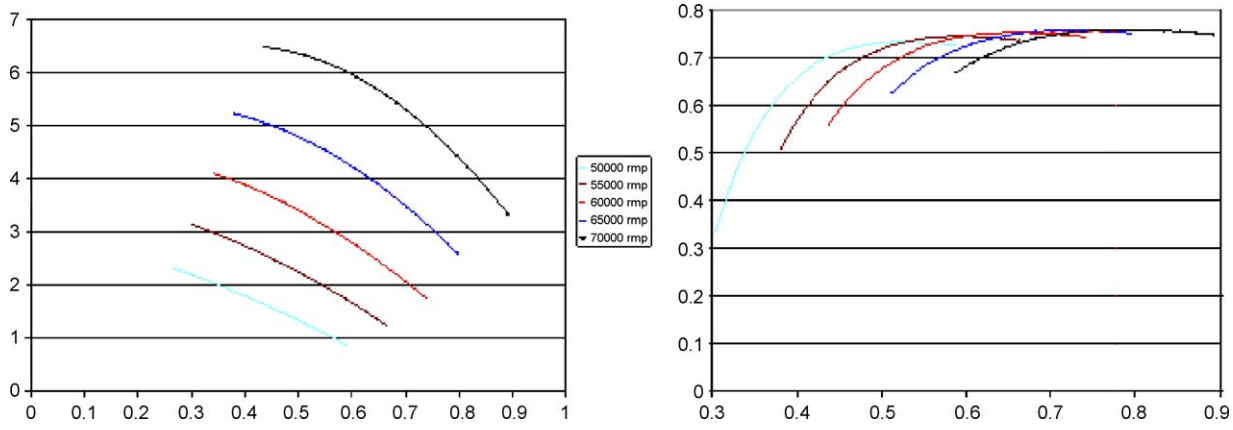

Fig. 3. Compressor's characteristics (β vs. kg s^{-1}; η vs. kg s^{-1}).

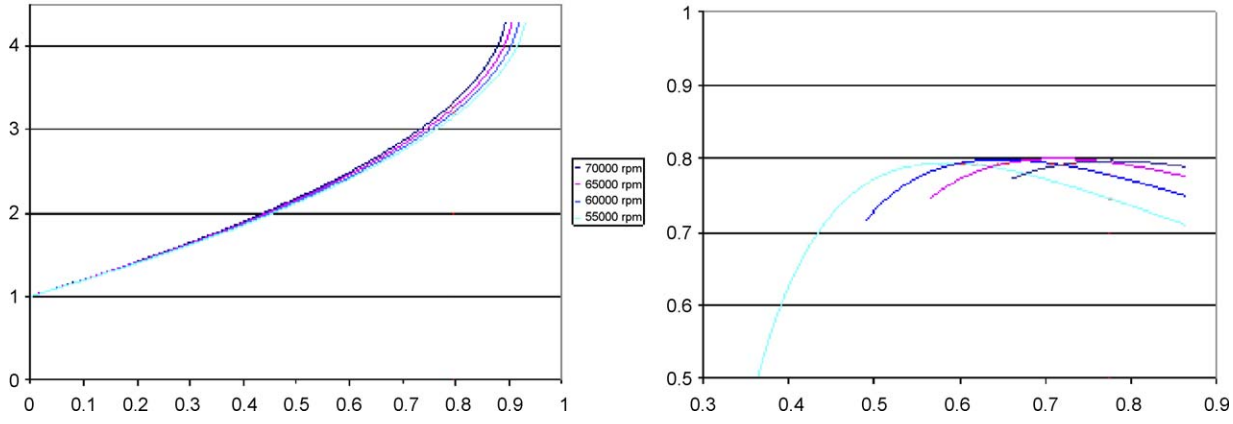

Fig. 4. Turbine's characteristics (β vs. kg s^{-1}; η vs. kg s^{-1}).

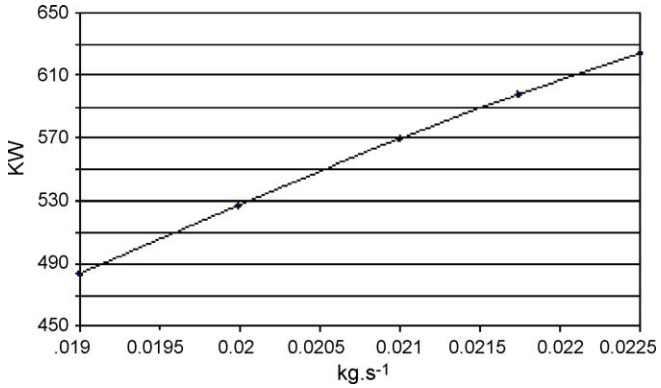

Fig. 5. Power produced vs. methane massflowrate.

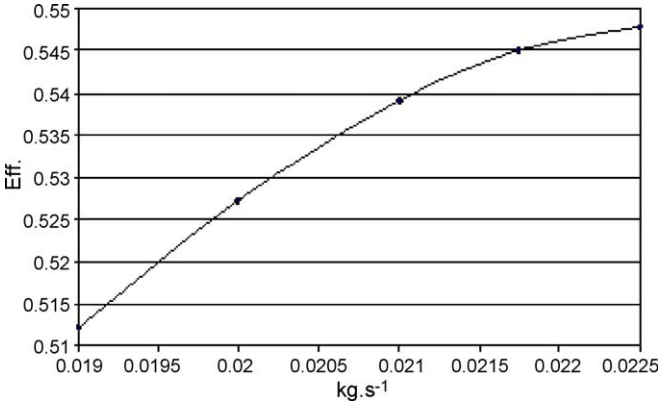

Fig. 6. Efficiency vs. methane massflowrate.

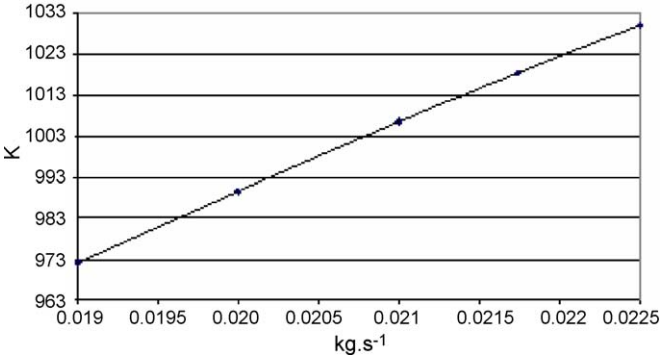

Fig. 7. Maximum local T vs. methane massflowrate.

included on the operating conditions forecasted by Ansaldo for the "Series 500" Demo Plant.

A fixed maximum local temperature of the solid parts of the cells (983 K) is obtained varying the input cathode gas temperature and flowrate. This constraint is necessary to reduce the electrolyte losses and corrosion phenomena. Cathode gas temperature and flowrate is controlled by adjusting the cathode inlet flowrate. This circumstance is obtained exploiting hot gas sensible heat, which raises the temperature of the fresh air, after mixing, varying the recirculation ratio and the air inlet. At the same time the air inlet have to guarantee the good matching between compressor and turbine maintaining high machines' efficiency. Another constraint is the steam to methane ratio: it must be over 3 to avoid the Boudouard reaction that would produce carbon which inhibits catalyst layer.

For a higher global efficiency, it is better to convert the energy inside the fuel cells stack, rather than in the turbine. Therefore, high fuel utilization is desired through the electrochemical device. On the other hand, diffusion phenomena have to be avoided, so H_2 and CO utilization in the stack up to 75% is selected. This value is obtained varying current density and methane feeding plant. A 443 K temperature was fixed for the steam at mixer with methane inlet, to assure after mixing a 408 K flow temperature (in fact at 350 kPa this is the necessary temperature to assure that steam does not condense). Considering the constraint explained in Table 6 an air mass flowrate of 0.683 kg s^{-1} was chosen and a recirculation ratio of 65%. In Figs. 3 and 4 are showed the compressor's characteristics and turbine's characteristics obtained by the model.

To choose the right methane mass flowrate a sensivity analysis was done varying the methane feeding plant and current density maintaining fuel utilization at 75%.

In Figs. 5–7 are shown the results obtained

As shown by Figs. 5 and 6 increasing the methane flow rate the power produced and the plant efficiency are improved but as showed by Fig. 7 the maximum local temperature is increased to value not tolerable by the fuel cell.

To have a fuel cell correct operation it is necessary therefore renounce to higher efficiency and choose lower methane flowrate.

In Table 7 are showed the input value chosen and the results obtained.

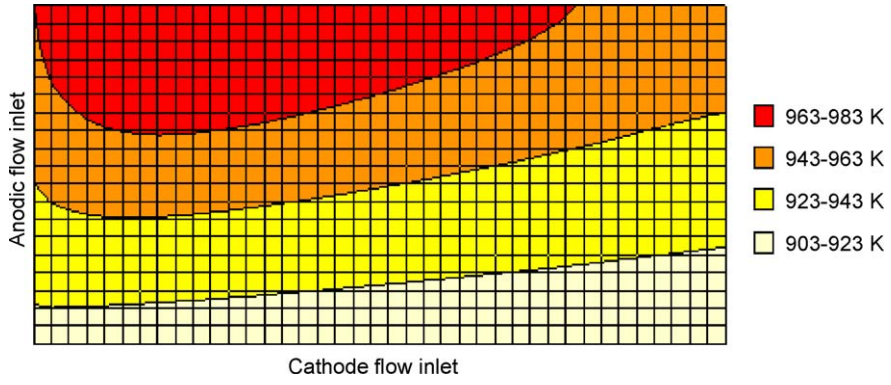

Fig. 8. Temperature map on the cell's plane.

Table 7
Input chosen and results

Air (kg s^{-1})	0.6833
Methane (kg s^{-1})	0.0196
Steam (kg s^{-1})	0.0722
Current density (A m^{-2})	1440
Power produced (kW AC)	516
Electrical efficiency (%)	52.7
Thermal power (kW)	212
Global efficiency (%)	74.3
Methane Conversion (%)	88.4

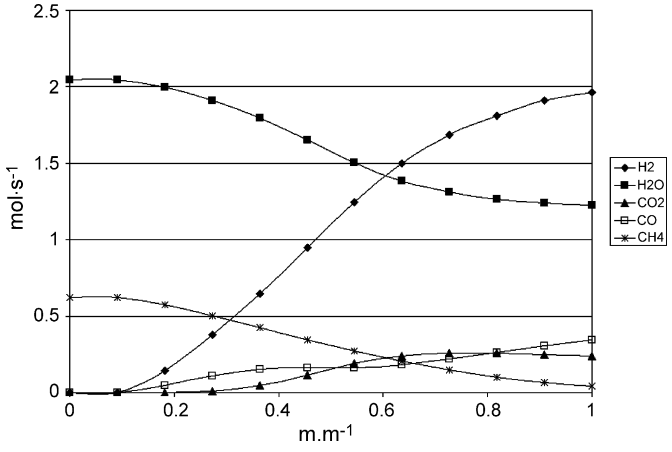

Fig. 9. Reaction progress in reformer.

Figs. 8 and 9 show instead the temperature map on the cell's plane and the hydrogen produced in the reformer side. The map shows that the cell's maximum temperature does not overreach 983 K.

3. Conclusion

The main steps of this work are

- The development of a fuel cell numerical model, implemented in Fortran 90, and interface whit Chemcad©.
- The development of a reformer/burner unit model employing in Fortran 90, and interface whit Chemcad©.
- The development of the turbine and compressor characteristic to completely define the behavior of the two machines.
- Assembling of a model for the complete system using the custom and Chemcad©library blocks.
- The study of the base case, driven on preliminary input specifications.

The simulation of the fuel cell has showed that global electrical efficiency surely can be kept easily over 50–55%, and a cogenerative efficiency about 75%. This result is due to the utilization of the microturbine that produce the necessary work for compressor and further energy. At the same time, the job has showed how the technologic barriers can reduce anyway the plant performance. This job showed anyway the symbiosis of the two machines (MCFC, gasturbine) and gets to first base for ulterior studies aimed to solve the problems that instead are emerged when the plant works at partial load.

References

[1] R.A. George, Status of tubular SOFC field unit demonstrations, J. Power Sources 86 (2000) 134.
[2] H. Maru, et al., Direct fuel cell/turbine hybrid system for ultra high efficiency power generation, Abstracts of the VII Grove fuel cell symposium, London, 2001.
[3] E. Liese, R.S. Gemmen, Dynamic modelling results of a 1 MW MCFC/GT power system, in: Proceedings of the ASME turbo expo 2002. Amsterdam, 3–6 June, 2002.
[4] G. De Simon, F. Parodi, M. Fermeglia, R. Taccani, Simulation of process for electrical energy production based on molten carbonate fuel cells, J. Power Sources 115 (2003) 210–218.
[5] B. Bosio, P. Costamagna, F. Parodi, Modeling and experimentation of molten carbonate fuel cell reactors in a scale-up process, Chem. Eng. Sci. 54 (1999) 2907–2916.
[6] J.M. Ogden, Review of small stationary reformers for hydrogen production. A report for the International Energy Agency agreement on the production and utilization of hydrogen Task 16, Hydrogen from Carbon-Containing Materials IEA/H2/TR-02/002.
[7] M. Zan, A. Gavriilidis, Catalytic combustion assisted methane steam reforming in a catalytic plate reactor, Chem. Eng. Sci. 58 (2003) 3947–3960.